Assessment of Vortex Induced Vibrations on wind turbines

Assessment of Vortex Induced Vibrations on wind turbines

Dimitris I. Manolas[1, 2], Panagiotis K. Chaviaropoulos[1], Vasilis A. Riziotis[2]

[1]iWind Renewables, PC, Kleisthenous 166 Gerakas, GR15344 Athens, Greece
[2]School of Mechanical Engineering, National Technical University of Athens, Heroon Polytechniou 9 Zografou, GR 15780, Athens, Greece

corresponding author's e-mail: d.manolas@iwind.gr

Abstract. Modern wind turbines are prone to Vortex Induced Vibrations (VIV). In the present work, an engineering semi-empirical framework is proposed that assesses VIV aero-elastic instabilities of wind turbine configurations. The procedure employs engineering tools relying on airfoil polars. It uses the state-of-the-art aero-elastic tool hGAST along with the EUROCODE VIV framework for steel structures extended to wind turbine configurations. The aero-elastic tool provides the missing modal input data (i.e. modal frequencies, total structural plus aerodynamic modal damping and modeshapes) to evaluate the semi-analytical expressions of the displacement and load amplitudes. Numerical results for single- and two-bladed configurations of the NREL 5MW Reference Wind Turbine (RWT) during assembly are presented, assessing turbine loads under the most unfavourable VIV scenarios examined.

1. Introduction

As the wind turbines are getting bigger in size, designs are becoming lightweight and consequently the ratio of the aerodynamic over the inertial loading increases. Advanced blade manufacturing processes increase the accuracy of construction and bill of materials, while they reduce blade's structural damping, which is further compromised by the more extended use of carbon composites. All the above, along with the increasing flexibility of modern designs that strengthen aero-elastic couplings and lower system natural frequencies, make wind turbines prone to Stall and Vortex Induced Vibrations (VIV). VIV is the aero-elastic instability a structure undergoes when the cross flow oscillating lift force, due to shedding of vortices, resonates with one of the system's natural frequencies. Severe VIV occur when the shed vortices form a coherent wake structure, which in wind turbines requires the rotor either locked or in idling mode. On the contrary, VIV are suppressed when the coherent structure of the shed vortices is destroyed, preventing vortex lock-on. Therefore, VIV rarely occur during normal operation but may appear under parked/idling conditions or during maintenance and assembly procedures. The question that needs to be answered by the manufacturers is whether the wind turbine is safe against VIV.

While the literature regarding VIV of cylindrical structures is rich, relevant experimental [1] or computational [2]-[6] works on wind turbine blades are scarce, attracting high attention the last decade. For a recent, detailed literature survey on VIV the reader is cited to [6]. Below we make reference to VIV studies on wind turbines (WTs). In early works VIV was studied on airfoil sections [2]-[4], while recent works by DTU consider the elastic blade clamped at its root [5]-[6]. In all the above references, free wake [2] or CFD [3]-[6] advanced aerodynamic methods were employed, primarily focusing on the aerodynamics of the complex VIV phenomenon either in stiff or

moving/elastic configurations. However, due to the complexity of the problem and of the high computational cost, none of the works assessed VIV of the entire (coupled) WT configuration.

In this work we present an engineering framework for performing VIV analysis of wind turbine configurations based on EUROCODE "VIV Approach 1" provisions [7]. This framework is incorporated in the aero-elastic tool hGAST [8]-[10] and relies on tabulated airfoil data (i.e. polars). Numerical results for single and two-bladed configurations of the NREL 5MW Reference Wind Turbine (RWT) [11] during assembly are presented, assessing turbine loads under the most unfavourable VIV scenarios examined. The paper is structured as follows; in section 2 the semi-empirical framework for VIV analysis is presented, in section 3 indicative numerical results are provided, while section 4 concludes the present work.

The contribution of the present work is the formulation of an engineering approach for wind turbines that allows performing VIV analysis of the entire (coupled) WT configuration. The engineering knowledge is combined with a state-of-the-art aeroelastic tool to assess turbine loads under the most unfavourable VIV scenarios, addressing excitation due to vortex shedding from the rotor or the tower at blade or tower frequencies. The established framework applies to all low damped modeshapes that may suffer from VIV, including 2nd tower modes in cases of tall towers with relatively low second tower frequency.

2. Methodology

The engineering semi-empirical framework for VIV analysis we establish in our present work is based on EUROCODE "Approach 1" [7] framework for steel structures, properly extended to wind turbine configurations including tower, nacelle, and rotor arrangements. It is incorporated in the non-linear, multi-body aeroelastic tool hGAST [8]-[10], in which both time-domain and eigenvalue stability analyses are available. In time-domain, hGAST applies the EUROCODE load as dynamic external force, while modal analysis provides all additional information needed (i.e. mode shapes, frequencies and total damping) to evaluate the semi-analytical expression of the displacement and load amplitudes. In the following sections we provide the background of EUROCODE approach, along with modelling assumptions and extensions made by the present work.

2.1. Baseline EUROCODE "VIV approach 1" for steel structures

Let $y(x,t)$ denote the displacement of a continuous elastic system (beam) in space-time coordinates. The modal representation of the above displacement field reads:

$$y(x,t)/D = \sum_{r=1}^{\infty} n_r(t)\varphi_r(x) \tag{1}$$

where $n_r(t)$ denotes the time varying modal coordinate or modal amplitude and $\varphi_r(x)$ the modeshape or modal function, while D is a characteristic length used for normalizing the displacement field.

The equation of motion governing the elastic problem in modal co-ordinates yields:

$$\ddot{n}_i(t) + 2\xi_i\omega_i\dot{n}_i(t) + \omega_i^2 n_i(t) = \frac{F_i(t)}{DM_i} \tag{2}$$

where ω_i and ξ_i are the modal frequency and modal damping ratio respectively of the ith mode, while M_i and $F_i(t)$ are the corresponding modal mass and modal force, defined as:

$$M_i = \int_0^l m(x)\varphi_i^2(x)dx = m_{ei}\int_0^l \varphi_i^2(x)dx \tag{3}$$

$$F_i(t) = \int_0^l f(x,t)\varphi_i(x)dx \tag{4}$$

where $m(x)$ is the linear mass per unit length, m_{ei} is the equivalent mass per unit length and $f(x,t)$ is the force per unit length.

In the simple case of a cantilever cylindrical beam of constant external diameter D, the VIV load can be defined as a sinusoidal crossflow lift force per unit length given by:

$$f(x,t)=\frac{1}{2}\rho V^2 D\Delta C_l\cos(\omega t) \tag{5}$$

where ρ is the air density, V is the wind speed, ΔC_l is the sinusoidal lift coefficient amplitude and ω the angular velocity. The elastic system gets into resonance as ω approaches one of its modal frequencies ω_i. When resonant lock-on conditions occur, vortices are shed coherently over a large area of the cylinder, the correlation length L_i referring to the i[th] mode. The RHS of the equation of motion (2) is then written as,

$$\frac{F_i(t)}{DM_i}=\frac{1}{2}\rho V^2\Delta C_l\cos(\omega t)\frac{1}{m_{ei}}4\pi K_w K=2\xi_i\omega^2\frac{1}{Sc}\frac{1}{St^2}K_w K\ \Delta C_l\cos(\omega t) \tag{6}$$

where K_w is the effective correlation length factor and K is the mode shape factor, given by [7]:

$$K_w=\int_{L_i}|\varphi_i(x)|dx\Big/\int_0^l|\varphi_i(x)|dx \tag{7}$$

$$K=\frac{1}{4\pi}\int_0^l|\varphi_i(x)|dx\Big/\int_0^l\varphi_i^2(x)dx \tag{8}$$

In the second expression in (6) the Strouhal (St) and the Scruton (Sc) numbers appear, defined as:

$$St=\frac{D\omega}{2\pi V} \tag{9}$$

$$Sc=\frac{4\pi\xi_i m_{ei}}{\rho D^2} \tag{10}$$

Following simple dynamic systems' theory, the maximum normalized displacement n_i at resonance is calculated as,

$$max(y_i/D)=\max(n_i)=\frac{1}{Sc}\frac{1}{St^2}K_w K\Delta C_l \tag{11}$$

The above expression is the formula provided by the EUROCODE for "Approach 1". It is noted that the maximum displacement increases with K_w suggesting that VIV is more pronounced when the coherent shedding takes place at the antinode of the considered modeshape, where the numerator of (7) attains its maximum. Moreover, the maximum displacement increases as the Scruton number gets lower, which, for a given aeroelastic system, happens when the total modal damping (structural, aerodynamic, soil, etc.), expressed through ξ_i, gets lower. In the opposite, an increased modal mass has stabilizing effect on VIV.

"VIV Approach 1" is applicable for any mode of generalized space frames consisting of beam elements due to its generality [7]. Its main drawback is that it lets all the VIV lock-on physics to be expressed through the semi empirical framework for L_i and ΔC_l, failing to comply with the strongly non-linear lock-on features that relevant experiments demonstrate.

The semi-empirical formulas suggested by EUROCODE for the calculation of L_i and ΔC_l are provided next for completeness. The non-dimensional correlation length, as a function of the maximum normalized displacement n_i, is given by,

$$\frac{L_i}{D}=min\left(max(4.8+12n_i,6),12\right) \tag{12}$$

whereas the oscillation lift amplitude ΔC_l is given by,

$$\Delta C_l=\min\left(max\left(3-2.4\frac{V_{crit,i}}{V_{m,Li}},0\right),1\right)C_{lat,0} \tag{13}$$

where $C_{lat,0}$ is the basic value of ΔC_l as given in Table E.2 of the EUROCODE, which for cylindrical bodies is assumed equal to 0.2 for the Reynolds numbers within [5 10^5 , 5 10^6], $V_{crit,i}$ is the critical wind velocity, given as a function of the Strouhal number and $V_{m,Li}$ is the mean velocity in the center of the correlation length L_i.

2.2. Additional negative aerodynamic damping term in VIV forcing term

In the following, we extend "Approach 1" theory with some successful features of "Approach 2". EUROCODE provides a second, more elaborate "Approach 2" for VIV calculations based on [12], the use of which is however restricted to the first mode of cantilever structures with a regular distribution of cross wind dimensions along the main axis of the structure. This approach allows for the consideration of different turbulence intensities, which may differ due to meteorological conditions. The essence of the theory behind "Approach 2" is the addition of an extra term to the aerodynamic force, which introduces negative aerodynamic damping when the structure starts vibrating because of vortex shedding. The aerodynamic force in equation (5) is then written as:

$$f(x,t)=\frac{1}{2}\rho V^2 D\ \Delta C_l \cos(\omega t)+2\ \omega_i\ \rho\ D^2 K_a \dot{y}(x,t)\left(1-G\dot{n}_i(t)^2\right) \tag{14}$$

where K_α is the aerodynamic damping coefficient, function of the Reynolds number, the geometry (cross section shape), the turbulence intensity and the stiffness of the structure, and G is a limiter of the negative damping term to avoid the system becoming unstable, so that $n_i(t)$ would never exceed a given value $(y/D)_{lim}$. Limiter G is given by:

$$G=\frac{4}{3}\frac{1}{\omega_t^2\left(y/D\right)_{lim}^2} \tag{15}$$

By introducing (14) in (2) and moving the additional (negative) damping term to LHS, the total damping term of the system is given by,

$$2\xi_i\omega_i\left[1-4\pi\frac{K_a}{Sc}\left(1-G\dot{n}_i(t)^2\right)\right]\dot{n}_i(t) \tag{16}$$

where all the remaining terms of the modal equation of motion (2) and the forcing term (6) remain unchanged. An approximate algebraic expression for $max(y_i/D)$ can be obtained for the derived non-linear dynamic equation using symbolic mathematics language.

In case no limiter is applied (i.e. $G=0$), the system becomes unstable when its total damping gets negative, which happens for $Sc \leq 4\pi K_\alpha$. However, this would not respect the physics of a dynamic system in resonance, whose extreme response is limited and not perpetually diverging.

In the above, one has still to calibrate the driving parameters L_i and ΔC_l but also K_α and $(y/D)_{lim}$. Nevertheless, this time L_i and ΔC_l do not have to include lock-on effects as the lock-on physics are now expressed in a phenomenological way through the limited damping term. Therefore, the L_i and ΔC_l values can be directly taken from aerodynamic (i.e. omitting the aero-elastic coupling) experiments or calculations. Also, the exact value of $(y/D)_{lim}$ is not that essential since one must prevent the structure entering in the negative damping region, which is signified by Sc and K_α, while the system's response around the critical Scruton number is insensitive to $(y/D)_{lim}$.

Higher turbulence levels reduce the critical Scruton $Sc_{crit}=4\pi K\alpha$ under which the vibrations get stronger. In this respect, K_α is expressed as $K_\alpha = K_{\alpha,max}\ h(TI)$, where TI expresses the fraction of the turbulence spectrum which lies above a characteristic for the structure length scale and $h(TI)$ is a declining function of TI. A simplified linear expression for h is $h(TI)=1\text{-}3TI$. For the range of application of "Approach 2", for circular cylinders and Reynolds numbers Re≥10^6, $K_{\alpha,max}=1$.

2.3. Extension to WT arrangements

Applying both "Approaches" to multiple turbine configurations with different number of blades and comparing vortex shedding results against an "equivalent" tower – lumped RNA analogue, it appeared that for unification reasons it was better to work with a modified Scruton number Sc^*, instead of the original Sc. This is because as additional bodies (blades) are considered in the system, m_{ei} but also K_w

values change drastically because their defining relations integrate the mode shapes along the added bodies as well. As a result, the bladed system and the equivalent RNA mass-lamped system would significantly differ in critical Scruton numbers (because of the m_{ei}) in the case of tower VIV, which is not reasonable. The modified Scruton is defined as,

$$Sc^* = Sc/(4\pi K_w K) \tag{17}$$

whereas (11) takes the form,

$$max\left(y_i/D\right) = \max(n_i) = \frac{\Delta C_l}{4\pi}\frac{1}{Sc^*}\frac{1}{St^2} \tag{18}$$

The critical Sc^* value becomes $Sc^*_{crit} = \beta K_a = \beta K_{a,max}(1-3TI)$, with $\beta = 1/(K_w K)$. For circular cylinders vibrating at their 1st mode $\beta \cong 13-15$.

Further, the above formulas have been obtained using the same characteristic length D to dimensionalize maximum displacement $max(y_i/D)$ and to define the Strouhal (St) and Scruton (Sc) numbers. In practice for the engineering semi-empirical framework established in the present work we needed to include blade/tower tapering and the case that vortex shedding springs from the blades but excites the tower modeshape. In this case, two distinct characteristic lengths should be considered, one for defining Strouhal denoted by C and another to dimensionalize the displacement denoted by D as previously. Then equation (18) for the maximum normalized displacement takes its final form,

$$max\left(y_i/D\right) = \max(n_i) = \frac{\Delta C_l}{4\pi}\frac{1}{Sc^*}\frac{1}{St^2}\frac{C^3}{D^3} \tag{19}$$

2.4. Assumptions and modelling details

Our basic assumption is that the well-known Crossflow or Independence Principle (IP) applies to wind turbine blades too. IP suggests that the yawed geometry, receiving the flow with an inclination angle, behaves like the normal-incidence case using the component of the free-stream velocity normal to the body axis. This is important in our case for coping with 2-bladed and 3-bladed configurations, where the 'Λ or V' blades see the flow with a ±60° inclination in respect to the blade stacking axis.

In Kaja et al. [13], the wake of tapered cylinders for certain inflow conditions accounted for a combination of two distinct shedding patterns (i.e., 2S and 2P). The lock-in regime of the reduced velocity for a tapered cylinder was found to be wider than that of a uniform cylinder. This is mainly because the variation of the local reduced velocity along the cylinder span increases the chance of lock-in, compared with the single reduced velocity in the uniform cylinder case. In addition, although the vortex shedding pattern may vary along the cylinder span, the frequencies of the vortex shedding and the sectional lift coefficient synchronize with the vibration frequency of the cylinder in the lock-in regime instead of varying along the cylinder span. Outside the lock-in regime, the flow pattern is like that of a single cylinder due to very small vibration amplitude. In our semi-empirical framework we apply the IP principle on tapered blade/tower geometries with the reduced velocity calculated using the mean characteristic length (chord or diameter) of the vortex shedding region.

The Strouhal number of the shed vortices depends on the cross section of the body. EUROCODE suggests St=0.18 for cylindrical cross sections but provides no value for airfoils. Horcas et al. [6] suggested a projected chord-based St number of 0.15-0.16 for inboard triggered vortex shedding. In an earlier work of ours [2] we have estimated St values for 2D airfoils in the range of 0.11-0.13, also reported in [3]. For the quantification of maximum displacements, we shall use St=0.15 for inboard shedding and St=0.12 for outboard shedding.

Lucor and Karniadakis [14] found that, for low Reynolds flows, the energy in the Strouhal peak disperses and decreases significantly with increasing inclination θ, whereas it is virtually submerged in the general wake turbulence spectrum for θ ≥ 60°. For θ = 60°, the rms values of the lift coefficient peak at the reduced velocity correspond to the largest cylinder response. Therefore, it seems that there is a loss of spanwise coherence and a drop in the correlation of the lift forces when the cylinder's response amplitude is maximum. We account for this effect in our semi-empirical framework by

reducing the coherence length of the inclined shedding area by 25% when θ = 60°, with the coherence length tending to zero as θ tends to 90° (currently applied only in case the rotor is considered locked).

In their paper Horcas and al. notice that at low inclination angles (0° to 10°) an unsteady turbulent wake dominates the flow, which is characterized by the shedding of disorganized vortical structures. When the inclination angle increases, stationary vortices are observed for a certain extent of the outboard part of the blade pointing towards the wind. The leeward vortices of this stationary wake are convected away from the blade following the flow direction forming a set of straight vortical tubes. At 70° inclination, the stationary wake is seen all along the blade span, remaining close to the body surface, while the shedding is only taking place in the vicinity of the blade root. In addition, the results of the flexible simulations of the baseline blade geometry showed significant edgewise vibrations for inclination angles between 47.5° and 60°. This lock-in condition between the fluid loading and the blade displacements was always accompanied by a reconfiguration of the stationary wake region into a parallel vortex shedding. This shedding was also observed at the tip vicinity, and it followed a 2S pattern.

Summing up for this tip effect it appears that a stiff blade in 'Λ or V' configuration with its tip pointing to the wind does not shed vortices from its tip region and one can make a similar hypothesis for the root region of its companion blade. Nevertheless, there is evidence that when VIV is triggered and the structure starts vibrating, this behaviour may change. For our purposes, and trying to avoid extreme conservatism, we shall assume that the two 'Λ or V' blades cannot shed vortices simultaneously both from their tip or their root region. The above assumption is further supported in case the rotor is free, by the fact that the two blades encounter different 2D projected velocities due to asymmetry in azimuth angle when the wind is coming from the side direction and the blades are pitched to feather position.

3. Numerical results and discussion

Numerical results for single- and two-bladed configurations of the NREL 5MW RWT [11] during assembly are presented using the established VIV simulation framework, assessing turbine loads under the most unfavorable VIV scenarios examined. The rotor is in idling mode (i.e. the brake is disengaged) and the blades pitched to feather position at 90°. Structural damping values of 0.19% and 0.25% are used for the tower and the blades respectively, significantly lower that the baseline values reported in [11], adapting to state-of-the art damping levels.

Table 1 provides the first and second stand still natural frequencies of the coupled NREL 5MW RWT configuration, equipped with one, two or three blades at 90° pitch, with free rotor (free-free drivetrain) and the gravity effect included. In the single- and the two-bladed configuration the rotor is analyzed at its static equilibrium state with the blades pointing downwards (one blade is vertical at 180° azimuth and two blades in 'Λ' position at 120° azimuth), while in the three-bladed configuration the first blade points upwards (0° azimuth). In the table, relative percentage differences are shown with respect to the three-bladed (full) configuration, which is included as a means of comparison although not analyzed.

Since the number of (first, second and higher) rotor modes per bending direction (i.e. flapwise and edgewise) should be equal to the number of the installed blade(s), one mode (symmetric) appears in the single-bladed case and two modes (symmetric and one asymmetric) in the two-bladed configuration per direction. Minor frequency differences are depicted that do not exceed 5% and 10% in the 2-bladed and 1-bladed configuration respectively. Expected tower frequency increase is depicted (~8% and 5%) in case one or two blades are equipped due to the reduced RNA mass. Higher frequency differences are seen in both first symmetric modes of the 1-bladed (about -10%) and 2-bladed (-4%) configurations, whereas the frequency difference of the remaining modes is marginal.

Modal analysis results define the modeshapes to be checked for VIV. The low damped first tower fore-aft and rotor edgewise mode(s) are expected to be prone to VIV when the blades are pitched to feather. Second modes of the analyzed configurations are too high in frequency to be excited at moderate to high wind speeds (2^{nd} tower frequencies ~2.8Hz), so they will not be included in VIV

analysis. In addition, modal analysis indicates the most effective for VIV shedding areas per modeshape. As mentioned in section 2 and demonstrated in Figure 1 for the single-bladed case (similar is the two-bladed case), shedding should be as close as possible to the antinode of the (excited) modeshape. In this respect, shedding from the tower top and the blade tip areas is expected to be worst case for the tower fore-aft and rotor edgewise mode(s) respectively. For tower mode excitation, two possible scenarios are considered, a) shedding from tower top and b) shedding from blade root.

Table 1: Stand still natural frequencies [Hz] of the coupled NREL 5MW RWT equipped with one, two and three blades with 90° pitch, free rotor and gravity included. Relative frequency differences with respect to the full (3-bladed) configuration are also provided.

	Modeshape	3-bladed	2-bladed		1-bladed	
1	1st tower fore-aft	0.32	0.33	5%	0.34	8%
2	1st tower side-side	0.32	0.33	3%	0.34	7%
3	1st rotor flapwise asymmetric 1	0.69	0.69	0%	-	-
4	1st rotor flapwise asymmetric 2	0.69	-	-	-	-
5	1st rotor edgewise asymmetric 1	0.88	0.88	0%	-	-
6	1st rotor edgewise asymmetric 2	1.02	-	-	-	-
7	1st rotor flapwise symmetric	1.04	1.00	-4%	0.94	-10%
8	1st rotor edgewise symmetric	1.16	1.11	-4%	1.06	-8%
9	2nd tower fore-aft	2.72	2.79	2%	2.78	2%
10	2nd tower side-side	2.88	2.88	0%	2.87	0%
11	2nd rotor flapwise asymmetric 1	1.97	1.97	0%	-	-
12	2nd rotor flapwise asymmetric 2	1.97	-	-	-	-
13	2nd rotor flapwise symmetric	2.04	2.03	-1%	2.01	-2%
14	2nd rotor edgewise asymmetric 1	2.77	2.79	1%	-	-
15	2nd rotor edgewise asymmetric 2	3.92	-	-	-	-
16	2nd rotor edgewise symmetric	4.08	3.99	-2%	3.93	-4%

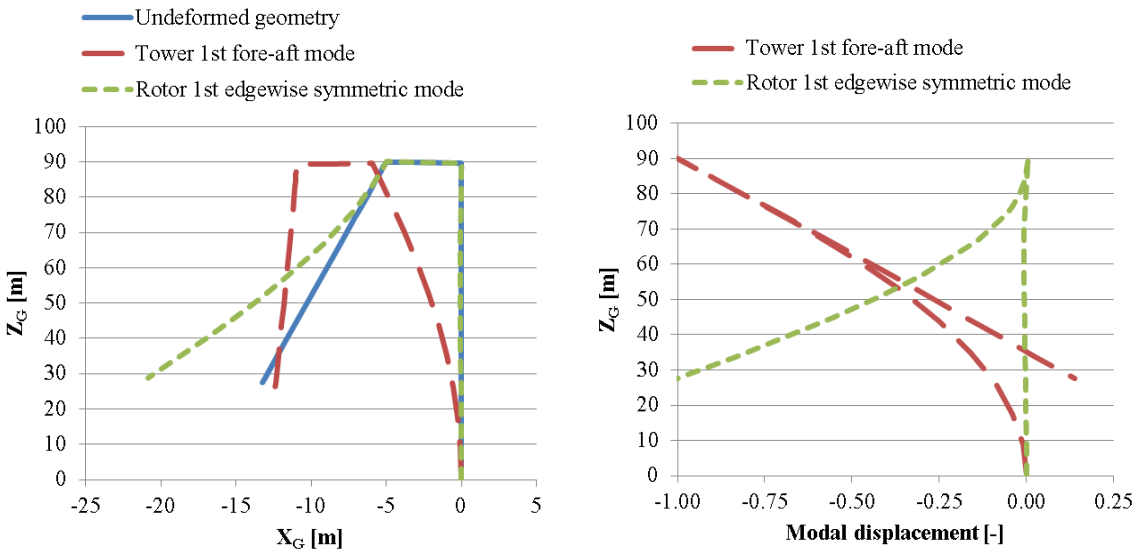

Figure 1: Low damped 1st tower fore-aft and 1st rotor (symmetric) edgewise modeshapes considered in VIV analysis of the NREL 5MW RWT single-bladed configuration; side view of the global 3D representation (left) and modal shape versus height indicating the antinodes at which modal displacement is maximum (right).

Before applying EUROCODE VIV semi-empirical framework, eigenvalue stability calculations are performed with the eigenvalue stability module of hGAST for various wind speeds for wind speeds in the range of 5m/s to 30m/s to obtain the modal characteristics of the low damped modeshapes of interest, namely the natural frequency, modeshape, steady state azimuth angle of the free rotor and total (structural plus aerodynamic) modal damping. Steady-state aerodynamics is assumed because for the yaw angles around ±90°, which are considered in VIV analysis we lack a reliable dynamic stall model to be used instead. Further, the effect of the vortex shedding is not taken into consideration. Steady wind inflow (i.e. no turbulence) with wind inclination of 8° and shear exponent of 0.11 has been selected.

Figure 2 shows the steady state azimuth angle of the two configurations, which gradually deviates from the equilibrium angle (i.e. 120° and 180° for the two- and single-bladed configuration respectively) as the wind speed increases. In both cases, it is seen that the rotor cannot rotate for any of the wind speeds considered with steady inflow (i.e. without turbulence).

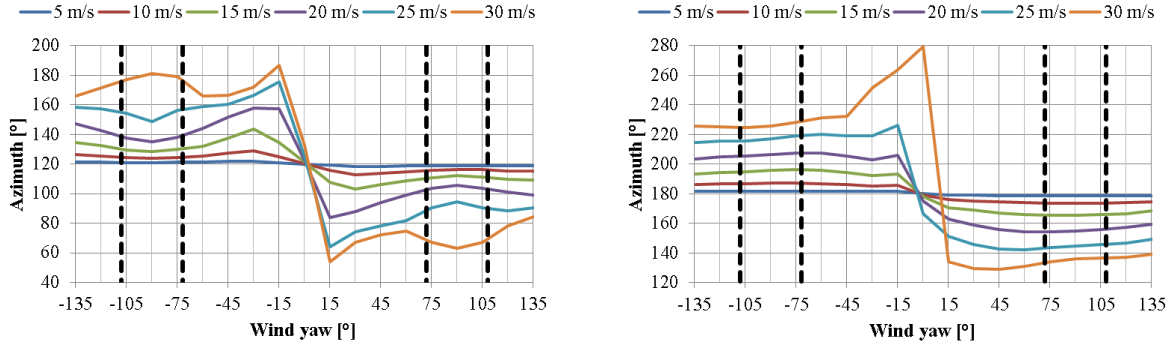

Figure 2: Rotor azimuth angle versus yaw of the NREL5 MW RWT two-bladed (left) and single-bladed (right) configurations for various wind speeds with free rotor, steady wind, wind inclination 8° and shear exponent 0.11, resulting from the eigenvalue stability analysis.

Figure 3 provides the total modal damping values for yaw angles around ±90°, which will be introduced in tabulated form in the VIV analysis semi-empirical framework. As indicated with the dashed black lines, we restrict the VIV analysis at flow conditions that the blades face the flow at angles of attach within the ranges [-105°, -75°] and [75°, 105°]. Similar damping values are estimated for the same modes of the singe- and the two-bladed configuration. Tower total modal damping is about 0.19-0.20%, almost insensitive to the wind speed variation, which means that the aerodynamic damping contribution is negligible. The aerodynamic damping contribution on the rotor edgewise asymmetric mode in the two-bladed case is small, as the total modal damping spans from 0.25% to 0.60% for the wind speeds considered. The rotor symmetric edgewise mode is higher damped as demonstrated through the increase of the damping values for increasing wind speeds. It should be noted that the variation of the azimuth angle of the free rotor introduces an inherent geometric non-linearity, so that damping levels are not linearly increasing with wind speed.

Results of the VIV analysis are presented in the next three tables. The 'VIV approach 1' is employed (i.e. K_α=0). It is reminded that shedding from one blade of the two-bladed configuration is only considered (the worst case is shown), whereas $\Delta C_l = 0.2$ and air density of 1.25kg/m^3 is assumed. Table 2 shows the input parameters of the worst VIV cases defined. *Case* is the type of shedding, first the body that sheds vortices and then the modeshape that is excited. For example B-T means shedding from the blade at the tower frequency, *Mode* is the excited mode, *Shedding* is the shedding body area of the assumed "worst case scenario" (where K_w is maximized), *St* is the imposed Strouhal number, *D* is the reference length (diameter or chord) used for the non-dimensionalization of the maximum oscillation deflection amplitude and *C* is the mean characteristic length of the shedding area.

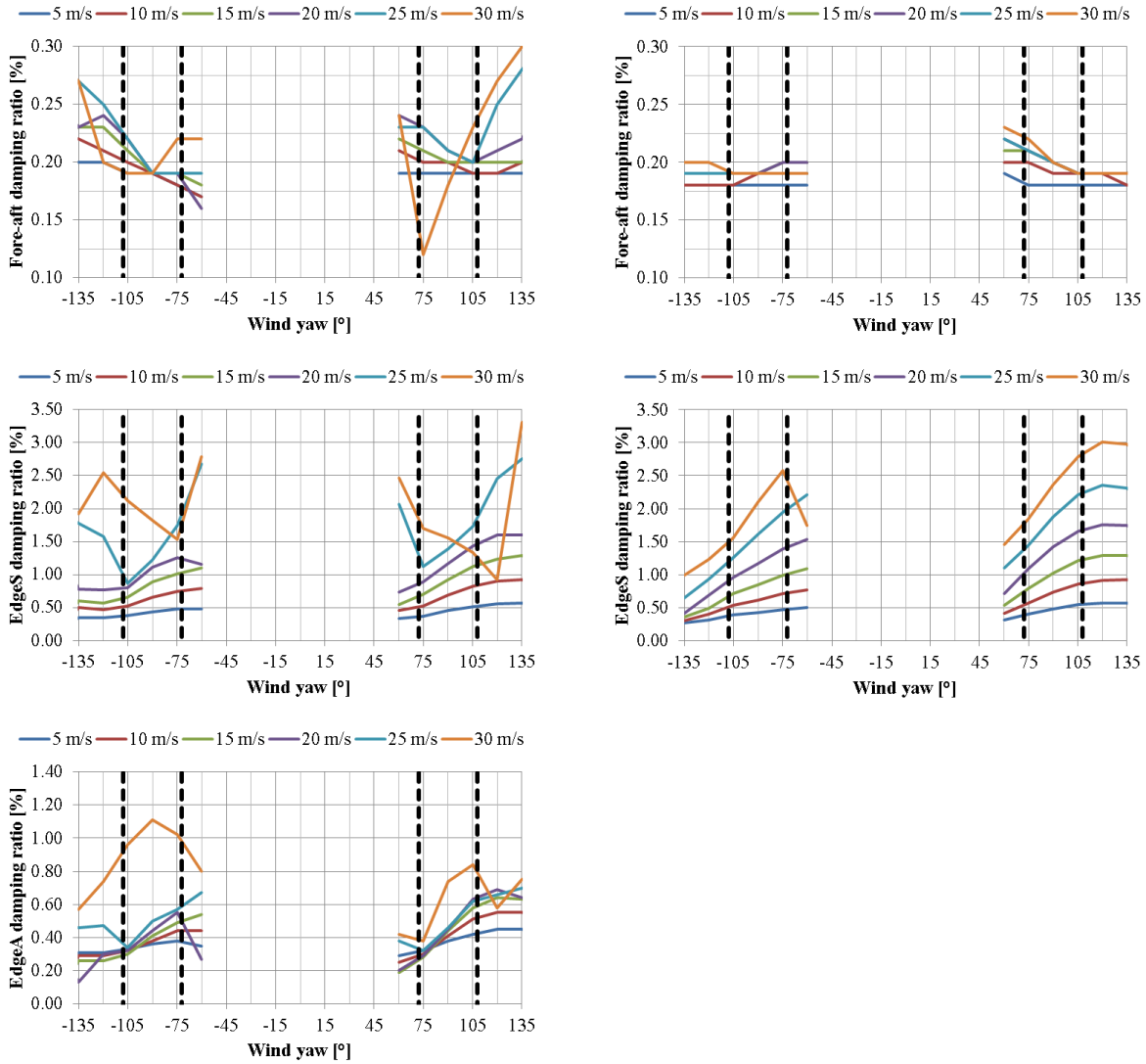

Figure 3: Total (structural & aerodynamic) modal damping ratio of the first fore-aft tower (top), rotor edgewise symmetric (middle) and rotor edgewise asymmetric (bottom) modes versus yaw of the NREL 5MW RWT two-bladed (left) and single-bladed (right) configurations for various wind speeds, resulting from the eigenvalue stability analysis with steady-state aerodynamics.

Table 2: Definition of the 'worst' cases and input parameters considered in VIV analysis.

ID [-]	Case [-]	Mode [-]	Shedding [-]	St [-]	D [m]	C [m]
1	T-T	fore-aft	Tower Top	0.18	3.87	3.87
2	B-T	fore-aft	Blade 1 Root	0.15	3.87	4.20
3	B-BA	edgeA	Blade 2 Tip	0.12	1.40	2.40
4	B-BS	edgeS	Blade 1 Tip	0.12	1.40	2.40

Table 3 and Table 4 provide the calculated modal quantities defined in the EUROCODE framework (see section 2 for their definition) and the output of the VIV analysis for the single- and the two-bladed configuration respectively. f and ξ denote the excited modal frequency and total damping ratio at the "worst case scenario" (minimum aerodynamic damping value within the considered yaw misalignment regime) derived through interpolation from the stability analysis results. *NL* is the non-

dimensional metric denoting the extent of the shedding area in characteristic length L multiples which derive through equation (12), m_e is the equivalent mass per unit length, K is the modeshape factor, K_w is the effective correlation length factor, while Sc and Sc^* denote the Scruton and the modified Scruton number respectively. V_{crit} is the Critical 2D cross sectional wind speed corresponding to the St number considered, V_{inf} is the actual wind velocity which projected on the shedding body (based on IP) yields V_{crit}, YAW_{inf} is the yaw misalignment of the "worst case scenario", $Azim$ is the azimuthal position of the free rotor and Y_{max} is the maximum combined oscillation deflection amplitude of the considered antinode.

It can be seen that apart from K all other modal quantities are significantly different between the two configurations. Specifically, K_W, m_e and Sc are almost double in the single-bladed configuration as compared to the two-bladed one. On the contrary, Sc^* values are very similar in case the oscillation amplitudes (Y_{max}) are close, justifying our choice to define it.

T-T case #1 represents tower excitation due to tower-top vortex shedding. The "worst case scenario" occurs for the single-bladed turbine at V_{inf}=7.3 m/s and YAW_{inf}=-105° and for the two-bladed configuration at V_{inf}=7.1 m/s and YAW_{inf}=-75°, whereas the maximum oscillation amplitude is 0.08 m and 0.07 m respectively. B-T case #2 represents tower excitation due to blade-root shedding. The "worst case scenario" for the single-bladed rotor occurs at V_{inf}=9.6 m/s (due to the difference in C_{ref} compared to case #1), while for the two-bladed setup at V_{inf}=14.7 m/s due to the projection of the inflow wind speed (based on IP), whereas YAW_{inf} is the same as case #1. The maximum oscillation amplitude of the single- and two-bladed case is 0.16 m and 0.18 m respectively. B-BA case #3 represents blade edgewise asymmetric mode excitation due to blade 2-tip shedding. The "worst case scenario" occurs at V_{inf}=17.6 m/s and yaw misalignment 75°, whereas the maximum combined oscillation amplitude is 2.61 m, a rather high value. Lastly, B-BS case #4 represents blade edgewise symmetric mode excitation due to blade-tip shedding. The "worst case scenario" occurs at yaw misalignment -105° and V_{inf}=28.5 m/s and 24.8 m/s for the single- and the two-bladed rotor respectively, whereas the maximum combined oscillation amplitude is 1.06 m and 1.34 m.

Table 3: VIV analysis results of the single-bladed NREL 5MW RWT configuration.

ID [-]	NL [-]	f [Hz]	ξ [%]	m_e [kg/m]	K [-]	Kw [-]	Sc [-]	Sc* [-]	V_{crit} [m/s]	V_{inf} [m/s]	YAW_{inf} [°]	Azim [°]	Y_{max} [m]
1	6.0	0.339	0.18	8087	0.13	0.27	9.8	23.1	7.3	7.3	-105	-	0.08
2	6.0	0.339	0.18	8087	0.13	0.29	9.8	21.0	9.5	9.6	-105	186	0.16
3	-	-	-	-	-	-	-	-	-	-	-	-	-
4	12.0	1.062	1.46	105	0.14	0.60	7.9	7.4	21.2	28.5	-105	222	1.06

Table 4: VIV analysis results of the two-bladed NREL 5MW RWT configuration.

ID [-]	NL [-]	f [Hz]	ξ [%]	m_e [kg/m]	K [-]	Kw [-]	Sc [-]	Sc* [-]	V_{crit} [m/s]	V_{inf} [m/s]	YAW_{inf} [°]	Azim [°]	Y_{max} [m]
1	6.0	0.332	0.18	3570	0.11	0.13	4.3	24.2	7.1	7.1	-75	-	0.07
2	6.0	0.332	0.19	3570	0.11	0.17	4.5	19.7	9.3	14.7	-75	129	0.18
3	12.0	0.879	0.30	121	0.13	0.39	1.9	2.9	17.6	22.2	75	218	2.61
4	12.0	1.112	0.87	97	0.15	0.39	4.3	5.7	22.2	24.8	-105	154	1.34

Figure 4 shows the spanwise distributions of the oscillating bending and deformation amplitudes of the worst VIV cases examined. Only the excited modeshapes are shown per component, thus tower signals correspond to tower mode excitation (VIV cases 1-2) and blade signals to rotor mode(s) excitation (VIV cases 3-4). Blade amplitudes due to tower excitation and tower amplitudes due to rotor mode(s) excitation are not shown, as for the analyzed configurations the couplings are insignificant and thus the amplitudes rather small.

It should be mentioned that it is out of scope of the present work to study whether the estimated load amplitudes are affordable or not and to examine the exact fatigue damage caused. Nevertheless, both tower cases (T-T and B-T) examined seem to be affordable and of low risk. The B-BS case could be considered of intermediate risk and alarming for low cycle fatigue damage as the oscillation amplitude of the blade moments is quite high for both configurations analyzed. Finally, the B-BA case, defined exclusively for the two-bladed rotor, is considered of high risk and very critical not only for fatigue damage but also for survival, as the oscillation moment amplitude approaches or even exceeds the ultimate design value. Consequently, the two-bladed configuration cannot be left unattended as it suffers from severe VIV.

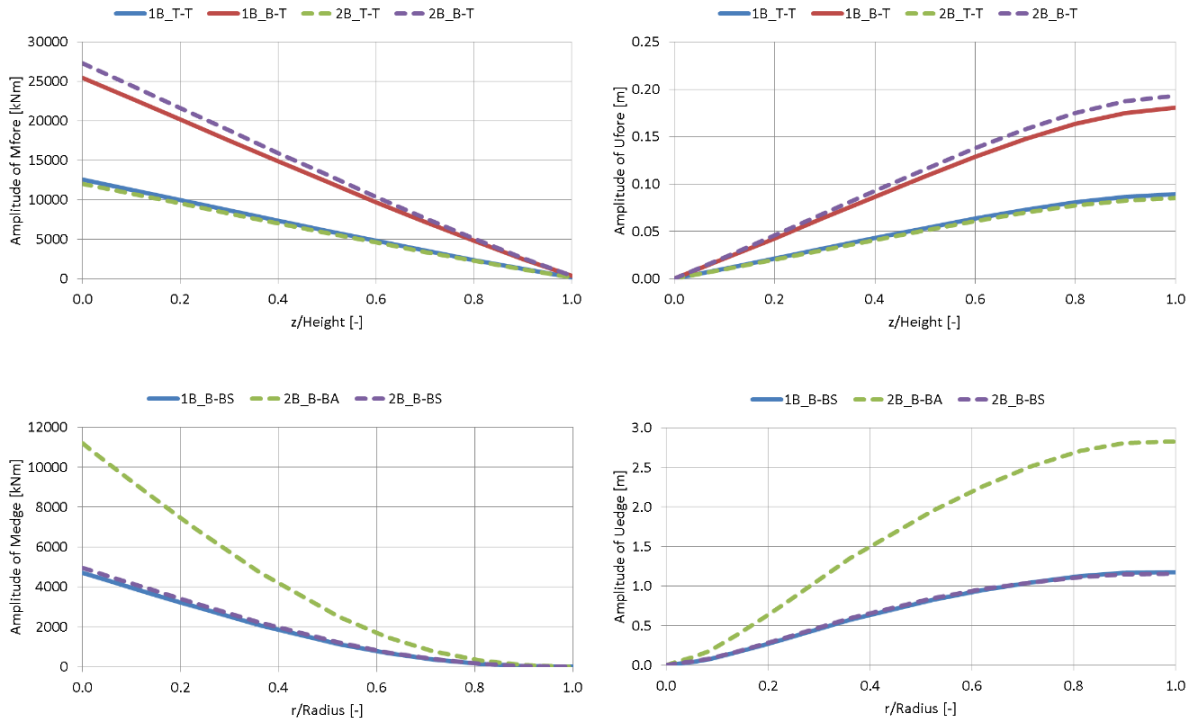

Figure 4: Spanwise tower (top) and blade (bottom) distribution of the oscillating moment (left) and deformation (right) amplitudes of the worst VIV cases examined of the single- and two-bladed NREL 5MW RWT configurations.

4. Conclusions

In the present work, an engineering semi-empirical framework was proposed to assess VIV aero-elastic instabilities of wind turbine configurations. It uses an extended implementation of EUROCODE "Approach 1" VIV framework for wind turbine configurations, which is incorporated in the state-of-the-art aero-elastic tool hGAST. The aero-elastic tool provides the modal input data needed to evaluate the semi-analytical framework. Numerical results for single- and two-bladed configurations of the NREL 5MW RWT during assembly were presented for the worst case VIV scenarios examined. The tower VIV cases examined were found to be affordable and of low risk, whereas the blade VIV cases are considered of intermediate (edgewise symmetric mode) and of high risk (edgewise asymmetric mode), as the oscillation amplitude of the blade edgewise moment is high.

It should be noted that EUROCODE VIV analysis method is trustful within the assumptions of the semi-empirical aerodynamic framework applied. In practice it is known that the method can be quite inaccurate providing less-conservative results when instabilities do exist and more conservative when they are absent. To increase confidence in the results, the aerodynamic framework needs further

adaptation and calibration, which is only possible through dedicated high fidelity aeroelastic analysis or experimental measurements.

The present engineering numerical framework can be used to efficiently scan a wide list of critical for VIV cases (e.g. all low damped modeshapes along with various critical shedding areas per mode), defined a-priori, and to provide valuable information about the critical inflow conditions and the corresponding oscillation load and deformation amplitudes. Various configurations prone to VIV might be considered, such as partially installed rotors during assembly and maintenance or parked turbines, as well as various pitch settings with locked or free drive-train. Even more important, although the procedure is subjected to the uncertainty due to the polars and the semi-empirical VIV framework, it can still be used in the design process to assess critical for VIV design parameters and to compare designs.

References

[1] Fontechaa R, Hennekea B, Kempera F and Feldmannb M 2017 Aerodynamic properties of wind turbine towers based on wind tunnel experiments *Procedia Engineering* **199** 3121–3126 DOI:10.1016/j.proeng.2017.09.557

[2] Zou F, Riziotis V A, Voutsinas S G and Wang J 2014 Analysis of vortex-induced and stall induced vibrations at standstill conditions using a free wake aerodynamic code *Wind Energy* **18** 2145-2169 DOI:10.1002/we.1811

[3] Pellegrino A and Meskell C 2013 Vortex shedding from a wind turbine blade section at high angles of attack *J. Wind Eng. Ind. Aerodyn.* **121** 131–137 DOI:10.1016/j.jweia.2013.08.002

[4] Skrzypiński W, Gaunaa M, Zahle F and Heinz J 2014 Vortex-induced vibrations of a DU96-W-180 airfoil at 90 angle of attack *Wind Energy* **17** 1495–1514 DOI:10.1002/we.1647

[5] Heinz J C, Sørensen N N, Zahle F, and Skrzypiński W 2016 Vortex-induced vibrations on a modern wind turbine blade *Wind Energy* **19** 2041–2051 DOI:10.1002/we.1967

[6] Horcas S G, Barlas T, Zahle F and Sørensen N N 2020 Vortex induced vibrations of wind turbine blades: Influence of the tip geometry *Phys. Fluids* **32** 065104 DOI:10.1063/5.0004005

[7] Eurocode 1: Actions on structures - Part 1-4: General actions - Wind actions EN 1991-1-4:2005

[8] Riziotis V A and Voutsinas S G 1997 GAST: A general aerodynamic and structural prediction tool for wind turbines *Proc. of the EWEC Conference* (Dublin Castle Ireland) pp 448–452

[9] Manolas D I, Riziotis V A, and Voutsinas S G 2015 Assessing the importance of geometric non-linear effects in the prediction of wind turbine blade loads *J. Comput. Nonlinear Dynam.* **10** 041008 DOI:10.1115/1.4027684

[10] Manolas D I, Riziotis V A, Papadakis G P and Voutsinas S G 2020 Hydro-servo-aero-elastic analysis of floating offshore wind turbines *Fluids* **5** 200 DOI:10.3390/fluids5040200

[11] Jonkman J M, Butterfield S, Musial W, and Scott G 2009 Definition of a 5-MW reference wind turbine for offshore system development National Renewable Energy Laboratory Golden, CO.

[12] Vickery B J and Basu R I 1983 Across-wind vibrations of structures of circular cross-section. Part I: development of a mathematical model for two-dimensional conditions *J. Wind Eng. Ind. Aerodyn.* **12** 49–73 DOI:10.1016/0167-6105(83)90080-6

[13] Kaja K, Zhao M, Xiang Y and Cheng L 2016 Three-dimensional numerical simulations of vortex-induced vibrations of tapered circular cylinders *Appl. Ocean Res.* **60** 1–11 DOI:10.1016/j.apor.2016.08.004

[14] Lucor D and Karniadakis G E 2003 Effects of oblique inflow in vortex-induced vibrations *Flow, Turbul. Combust.* **71** 375–389 DOI:10.1023/B:APPL.0000014929.90891.4d